

Article

Experimental Study on Evaporation and Micro-Explosion Characteristics of Ethanol and Diesel Blended Droplets

Yixuan Zhang¹, Kesheng Meng^{2,3}, Lin Bao², Qizhao Lin^{2,*} and Svitlana Pavlova^{1,*} ¹ School of Software, Shanxi Agricultural University, Jinzhong 030801, China; zhangyixuan1230707@163.com² Department of Thermal Science and Energy Engineering, University of Science and Technology of China, Hefei 230026, China; mengkesheng@126.com (K.M.); baolin@mail.ustc.edu.cn (L.B.)³ Department of Aviation, Anhui Communications Vocational & Technical College, Hefei 230051, China

* Correspondence: 18255107780@163.com (Q.L.); pavlova_2020@ukr.net (S.P.)

Abstract: In this study, the constant temperature control system of a heating plate was established, ethanol–diesel fuel with different proportions was prepared, and a series of experiments were carried out. The experimental system was used to observe, summarize, and analyze four evaporation and crushing modes of mixed droplets, which were explosion, liquid filament stretching, exocytosis, and ejection mode. The evaporation process of four kinds of mixed droplets in their life cycle was analyzed by normalizing the diameter square. It was proposed that the evaporation process of droplets could be divided into the following three stages: a heating stage, a fluctuating evaporation stage, and an equilibrium evaporation stage. It was also pointed out that the expansion, ejection, and micro-explosion of droplets were the causes of fluctuating evaporation. The concept of expansion and crushing intensity was put forward and the expansion and crushing intensity of ethanol/diesel mixed droplets with different proportions were calculated. The reasons why expansion and crushing intensity first increased and decreased with the increase in ethanol blending ratio were analyzed. Finally, the time proportion of ethanol–diesel mixed droplets in each evaporation stage was calculated, which explained that the time proportion of the instantaneous heating stage showed a parabolic law with the increase in ethanol content.



Citation: Zhang, Y.; Meng, K.; Bao, L.; Lin, Q.; Pavlova, S. Experimental Study on Evaporation and Micro-Explosion Characteristics of Ethanol and Diesel Blended Droplets. *Atmosphere* **2024**, *15*, 604. <https://doi.org/10.3390/atmos15050604>

Academic Editor: Kenichi Tonokura

Received: 11 April 2024

Revised: 7 May 2024

Accepted: 13 May 2024

Published: 15 May 2024



Copyright: © 2024 by the authors. Licensee MDPI, Basel, Switzerland. This article is an open access article distributed under the terms and conditions of the Creative Commons Attribution (CC BY) license (<https://creativecommons.org/licenses/by/4.0/>).

Keywords: ethanol; diesel; evaporation model; micro-explosion; intensity

1. Introduction

According to the data of the BP World Energy Outlook (2020) [1] and the International Energy Agency, crude oil accounts for nearly 40% of primary energy; liquid fuel is still the main energy source in today's society and the large consumption of liquid fuel will inevitably lead to increased pollutant emissions. Replacing diesel with ethanol [2] with a higher oxygen content can reduce the dependence on fossil fuels and reduce the emission of greenhouse gases and other harmful gases. However, the single use of ethanol is limited by the yield and food security. Adding a certain proportion of ethanol to diesel oil can significantly reduce pollutant emissions [3–7] and delay the depletion of fossil fuels [8,9].

A series of complex physical and chemical phenomena, such as expansion [10,11], ejection [12], and micro-explosion [13–18], can occur during the combustion of blended fuels, among which micro-explosion is the most representative. Micro-explosion means that mixed droplets are heated to a certain time at high temperatures and suddenly burst into micro-droplets with different volumes. According to the micro-explosion time of the droplet and the number of micro-droplets after micro-explosion, micro-explosion can be divided into five types of micro-explosion with different intensities [19]. Homogeneous nucleation and heterogeneous nucleation theory [20,21] can be used to explain the process of micro-explosion. By using this theory, the overheating limit model of mixed droplets was established and it was pointed out that the micro-explosion intensity of droplets with uniform nucleation was greater than that of droplets with non-uniform nucleation [22,23].

An ethanol–diesel fuel mixture can produce expansion, ejection, and micro-explosion events [24,25] during heating, which can improve the evaporation rate [26,27] and combustion efficiency [24,28]. Wang et al. [29] studied the evaporation characteristics of soybean oil droplets and found that the micro-explosion intensity of droplets produced via uniform nucleation was higher than that of non-uniform nucleation, and the higher the micro-explosion intensity, the faster the evaporation rate. Hallett et al. [30] conducted an experimental study on the evaporation of emulsified ethanol–diesel oil droplets. During the experimental process, the sharp ejection phenomenon of droplets was observed and many micro-sub-droplets were sputtered from the main droplets. The ejection phenomenon caused by droplets reduced the droplet size and ignition delay time. Wang et al. [31] studied the micro-explosion and evaporation characteristics of nano-fuel droplets and found that with the increase in cerium oxide concentration, the micro-explosion delay time gradually decreased. Mikami et al. [32] pointed out that micro-explosion was the cause of the destructive combustion of droplets and the occurrence time of micro-explosion was mainly distributed during quasi-steady evaporation. Under certain environmental pressures, the micro-explosion intensity of droplets was mainly affected by environmental temperature. The higher the environmental temperature, the higher the micro-explosion intensity, the greater the possibility of micro-explosion, and the shorter the delay time of micro-explosion. Meanwhile, the environmental pressure [33,34] had an important influence on the combustion characteristics of droplets. With the increase in environmental pressure, the evaporation rate and micro-explosion intensity of droplets decreased. Homogeneous nucleation and heterogeneous nucleation theory [22,35,36] were important theories to explain the occurrence process of micro-explosion phenomenon of mixed droplets. Zhang et al. [22] established a mathematical model to predict the overheating limit of aqueous ethanol–diesel emulsion by using molecular dynamics theory and verified the model. It was found that the micro-explosion intensity of the uniform nucleation of water–ethanol–diesel emulsion droplets was greater than that of non-uniform nucleation, and eliminating the non-uniform nucleation sites in combustion droplets could prevent micro-explosion [23].

The micro-explosion phenomenon exists in the process of the spray combustion of diesel engines [37], and the micro-explosion of droplets promotes atomization and evaporation [38–40]. The higher the micro-explosion intensity of mixed droplets during heating, the greater the evaporation rate of droplets. M. A. et al. [39] studied the spray characteristics of diesel oil and water emulsions at high temperature and high pressure and found that droplets with a diameter of less than 50 microns produced a weak micro-explosion, which was related to the size of droplets and significantly affected the atomization of fuel. The higher the micro-explosion intensity of droplets, the more secondary droplets were formed, the more thoroughly the droplets were destroyed, and the faster the droplets evaporated [41,42]. In addition, it was pointed out that the more components of mixed fuel, the faster the evaporation rate [38,43,44]. Taking diesel, biodiesel, and ethanol as examples, the relationship of evaporation rates was as follows: diesel oil < diesel oil + biodiesel < diesel oil + biodiesel + ethanol.

Researchers had shown great interest in the use of blended fuels and had conducted a lot of research on engines, high-pressure common rail systems, and constant volume bombs, which mainly focused on engine emissions, power, and single droplet micro-explosion, but the research on the evaporation, micro-explosion of mixed droplets, and their relationship was rare. Based on previous research [19,45,46], it was observed that the evaporation of ethanol–diesel droplets could be divided into the following three stages: instantaneous heating, fluctuating evaporation, and equilibrium evaporation. Different micro-explosion modes of ethanol–diesel droplets and their intensity relationships were studied and the expansion and crushing intensity of ethanol–diesel droplets were calculated, which provided a basis for the use of alternative fuels.

2. Experimental Device and Image Processing Method

2.1. Evaporation Device

A schematic diagram of the experiment is shown in Figure 1a; it mainly included a high-speed photography system, a heating system, an automatic guide rail, and a data acquisition system. The main experimental equipment is shown in Figure 1b. The wire, with a diameter of 0.15 mm, was a Cr/Ni alloy (Cr20/Ni80), with lower thermal conductivity ($15 \text{ W/m}\cdot\text{k}$) compared with cast iron ($55 \text{ W/m}\cdot\text{k}$), aluminum ($237 \text{ W/m}\cdot\text{k}$), and copper ($401 \text{ W/m}\cdot\text{k}$). Cr-Ni wire was selected because of its lower thermal conductivity and strong adhesion properties. Initially, the Cr/Ni alloy wire (Cr20/Ni80) was selected based on its well-documented low thermal conductivity, typically cited as $15 \text{ W/m}\cdot\text{K}$ in the materials science literature. To ensure the accuracy of this value under our specific experimental conditions, we conducted comparative measurements using standard thermal conductivity measurement techniques, such as the guarded hot plate method or laser flash analysis. The values obtained were consistent with the literature. Mura et al. [47] pointed out that a Cr-Ni thermocouple did not affect the micro-explosion of water–diesel emulsified droplets. In addition, this paper mainly investigated the evaporation and micro-explosion characteristics of mixed droplets of ethanol and diesel at different ratios; the micro-impact on mixed droplets at each ratio was the same, so the analysis of the conclusion using nickel wire was reliable.

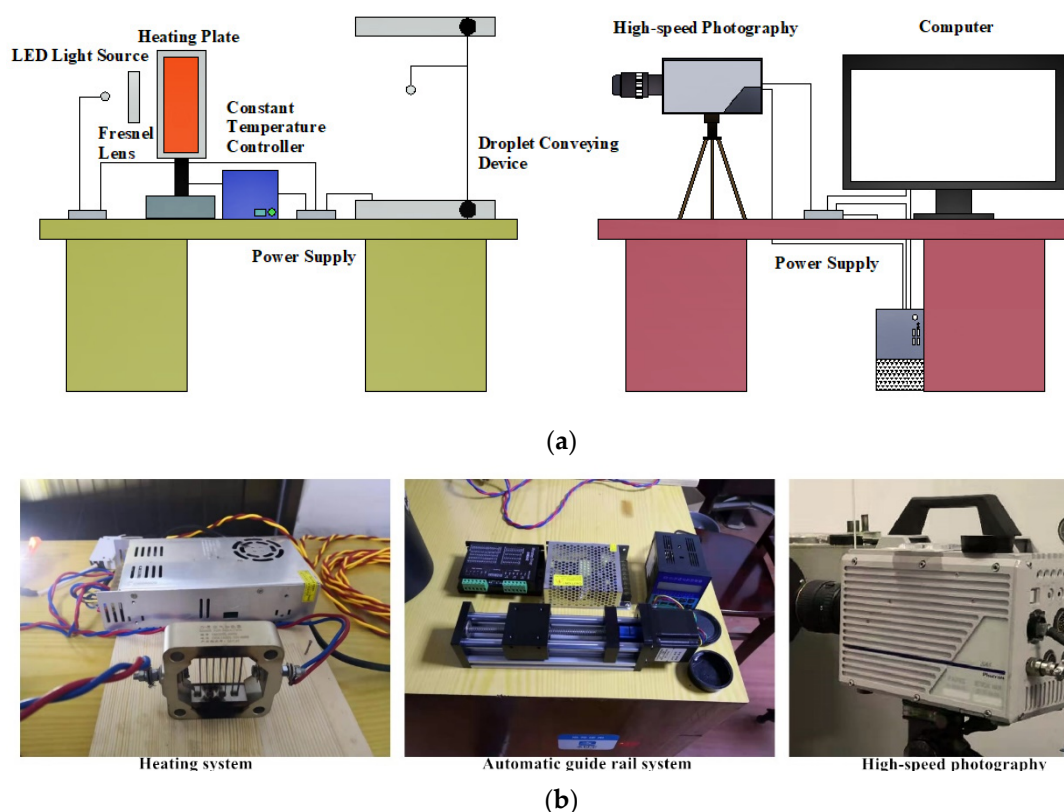


Figure 1. (a) Schematic diagram of experiment. (b) The main experimental equipment.

In the high-speed photography system, the frame rate of the high-speed camera (From China Canon EOS 7D Mark II, with EF70-200mm F2.8 USM IS camera lens) was set at 2000 fps, and the exposure time was $1/2000 \text{ s}$. In front of the camera lens, an LED light source with a power of 80 w, which generated parallel light, was placed to ensure the amount of light entering the lens. The main equipment of the heating system was an air heater. The heating temperature was set at 723 K. A thermocouple connected with the temperature controller was placed 0.2 mm in front of the heating plate. The thermocouple was used to measure the temperature there and the error range of the thermostatic controller

was 2 k. The moving speed of the automatic guide rail was set to 1 m/s, the distance between the initial position and the preset position was 0.2 m and the conveying time was 0.2 s. Each experimental condition was tested three times to ensure reliability in our observations. The pictures obtained using high-speed photography were transmitted to the computer through the data acquisition system for subsequent processing.

2.2. Image Processing Method

The time chart of the evaporation process of mixed droplets was recorded using a high-speed photography system and the image was processed using the MATLAB program. The stage of the MATLAB algorithm is shown in Figure 2; it mainly includes five stages such as cutting, color scale processing, and open and close operation, where (a) represents the original image, (b) represents the cropped image, (c) represented a color-scale picture, (d) represented a black and white image, (e) represented a binary image, and (f) represented the equivalent circle image. The moment when the guide rail transports the droplet to the first picture at the set position was defined as the evaporation start time, and the droplet size at this time was the initial size, and its diameter was calibrated as being equivalent to 1. To reduce the amount of calculation in the image processing process, first, observe the distribution area of mixed droplets in all pictures, cut out the target area, then take the burnt-out image as the base image, set the gray threshold, divide the area where the droplets were located by other areas, and calculate the pixel number of the droplet area. By subtracting the pixel number of fibrils in the base picture, the actual pixel number of the droplet projection was obtained. The number of pixels was converted into the actual area, according to the ratio measured using experiments, and was then converted into the diameter of the circle with equal area and was compared with the initial droplet diameter, whereby the equivalent ratio change of the droplet diameter was obtained.

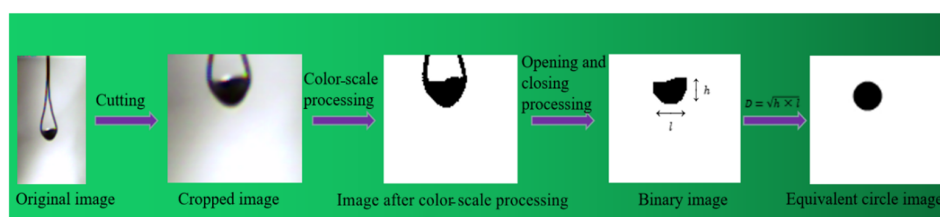


Figure 2. The stages of the MATLAB algorithm.

2.3. Fuel Preparation and Physical Properties

The miscibility between ethanol and diesel oil was poor, and the stability and uniformity of the mixed fuel produced by ethanol and diesel were poor. Adding a certain amount of n-decanol could significantly improve the mixing uniformity of ethanol and diesel. Therefore, in this paper, n-decanol was selected as cosolvent and all the materials were prepared according to the volume fraction, including 20% ethanol + 78% diesel + 2% n-decanol (DE20), 40% ethanol + 58% diesel + 2% n-decanol (DE40), 60% ethanol + 38% diesel + 2% n-decanol (DE60), and 80% ethanol + 18% diesel + 2% n-decanol (DE80). The addition of a cosolvent exerts a minimal effect on the evaporation and micro-explosion of the mixture; therefore, we have deliberately limited the cosolvent content to just 2% in this experiment. Furthermore, the use of a consistent volume of cosolvent across all blends was to ensure uniformity in this minimal influence, thereby not affecting the analysis of trends in evaporation and micro-explosion characteristics. The components and names of experimental fuels are shown in Table 1 and some properties of biodiesel and ethanol are shown in Table 2.

Table 1. Composition and name of fuel blends.

Composition of Fuel Mixture (Volume Basis)	Designated Nomenclature
20% ethanol, 78% diesel, 2% n-decanol	DE20
40% ethanol, 58% diesel, 2% n-decanol	DE40
60% ethanol, 38% diesel, 2% n-decanol	DE60
80% ethanol, 18% diesel, 2% n-decanol	DE80

Table 2. Properties of test fuels.

Properties	Diesel	Ethanol	DE20	DE40	DE60	DE80
Density (20 °C) [kg/L]	0.822	0.789	0.816	0.811	0.805	0.799
Viscosity (20 °C) [mm ² /s]	2.93	1.20	1.95	1.82	1.72	1.63
Surface tension (mN/m)	27.84	22.32	23.41	23.25	23.09	22.98
Boiling point (K)	550–650	351	—	—	—	—

To obtain different proportions of ethanol–diesel droplets, a microliter syringe with a measuring range of 5 microliters was used in this experiment, as shown in Figure 3. Using this microliter syringe, different proportions of 1.5 microliter ethanol–diesel mixed droplets were obtained. In the experimental setup, we utilized anhydrous ethanol with a purity of 100% to ensure consistent results across tests. This level of purity was critical, considering ethanol’s role in the studied evaporation and combustion processes. The use of highly pure ethanol eliminates variability that could arise from impurities, allowing for a precise assessment of ethanol’s effects in the fuel blend.

**Figure 3.** The microliter syringe with a measuring range of 5 microliters.

3. Results and Discussion

3.1. Evaporation Sequence Diagram of Mixed Droplets

3.1.1. Evaporation Sequence of the DE20 Droplet

The evaporation sequence diagram of the DE20 droplet is shown in Figure 4. After being transported to the designated position by the digital guideway system, the DE20 droplet underwent a stable endothermic process, during which the volume of the droplet remained relatively unchanged. At 5.59 ms/mm², the droplet began to burn. Although no ethanol vapor escaped during this period, it could be inferred that the temperature of the droplet reached the boiling point of ethanol during heating, and a small amount of ethanol began to evaporate and escaped from the top of the droplet. During combustion, the droplet was heated rapidly and a large amount of heat was accumulated inside the droplet. In addition, the temperature increased sharply and the light components (ethanol) in the droplet gradually gathered. At 8.18 ms/mm², an extremely fierce explosion occurred and the whole droplet splashed out at the contact with the filament, forming a main droplet and a large number of sub-droplets. Because of the high micro-explosion intensity, the main droplet first expanded into a plane shape and gradually shrank under the influence of surface tension, while the sub-droplets burned quickly after being separated from the main droplet, which was beneficial to shorten the ignition delay time of fuel and accelerated the combustion in actual working conditions. At the time of 8.39 ms/mm², the droplet

had fused into spheres and there were a lot of bubbles in the droplet, so the volume of the droplet expanded. On the one hand, the local temperature rose due to the burning of sub-droplets after the droplet burst, the main droplet absorbed a lot of heat from the environment, and the internal temperature had reached the overheating limit of ethanol, and some ethanol evaporated. On the other hand, the surrounding air was sucked in the process of droplet fusion, which made the droplet expand. This showed that the occurrence of micro-explosions was beneficial to the mixing of oil and gas and then made the fuel burn completely. In the following period, the vaporized fuel was sputtered out of the droplet, the volume of the droplet gradually decreased, and the droplet also started to shrink. At 8.70 ms/mm², the sub-droplet also produced a micro-explosion, which further proved that small-sized droplets could also produce micro-explosions. After micro-explosion, the droplets expanded rapidly and sputtered at 9.11 ms/mm². The sputtered fuel burned rapidly in the environment and produced a flame. At 9.15 ms/mm², the droplets were stretched into filaments, which were broken by gravity and merged at 9.27 ms/mm². On the one hand, the droplet was stretched into filaments because of the deformation caused by sputtering and, on the other hand, the nucleation points in the droplets were roughly distributed in a straight line and the droplet was stretched into long strips.

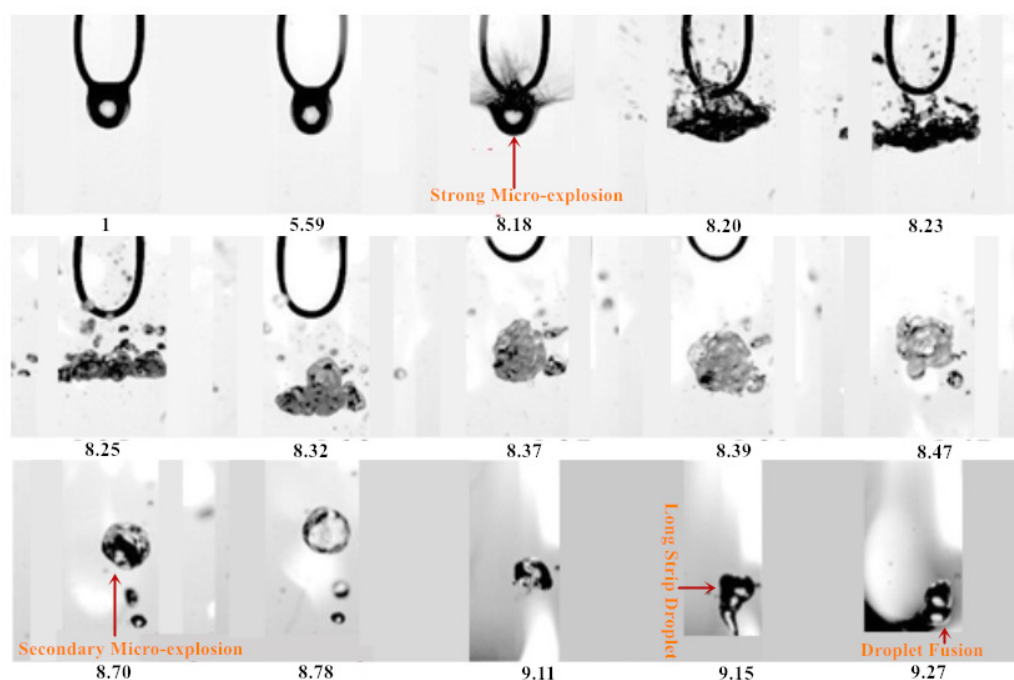


Figure 4. The evaporation sequence diagram of the DE20 droplet.

3.1.2. Evaporation Sequence of the DE40 Droplet

The evaporation sequence diagram of the DE40 droplet is shown in Figure 5. After being transported to the designated position, the DE40 mixed droplet also experienced a stable endothermic stage, but, at the time of 3.72 ms/mm², a small bubble appeared on the left side of the droplet. At 4.09 ms/mm², the bubble moved to the upper left of the droplet and began to expand. The vaporized ethanol vapor accumulated on the left side of the droplet, and, at the time of 4.44 ms/mm², part of the ethanol vapor broke through the liquid film and escaped from the droplet, resulting in an ejection phenomenon. At the time of 4.80 ms/mm², the droplet volume expanded to the maximum value and an obvious weak area of liquid film appeared in the lower left corner of the droplet. At 4.82 ms/mm², a crater was formed at the lower left of the droplet surface, from which gas escaped. Although there was a big gap on the surface of the droplet, only some small droplets were observed to be ejected from this place. Because it was very similar to cell exocytosis, it was called exocytosis. A higher-intensity microburst occurred in E20 and

a lower-intensity microburst occurred in DE40. During the E20 droplet micro-explosion process, the primary droplets produced a large number of secondary droplets, while the DE40 droplet micro-explosion process produced fewer secondary droplets. The reason why mixed droplets produce micro-explosions of different intensities mainly depends on the vapor pressure in the bubbles. The greater the vapor pressure, the more complete the bubble bursts. The more secondary levels are generated, the higher the micro-explosion intensity. After exocytosis, the droplet was affected by a great recoil force and underwent great deformation and shrank into liquid nuclei, and the escaping gas burned near them. At 5.26 ms/mm^2 , the droplet produced exocytosis again and was deformed under the impact of reaction force. The exocytosis appeared again at 6.22 ms/mm^2 , but it happened in the upper right corner of the droplet. The exocytosis occurred after the expansion of droplet, which was accompanied by mass transfer. Light components gradually gathered in the weak area of liquid film and steam escaped from the crater.

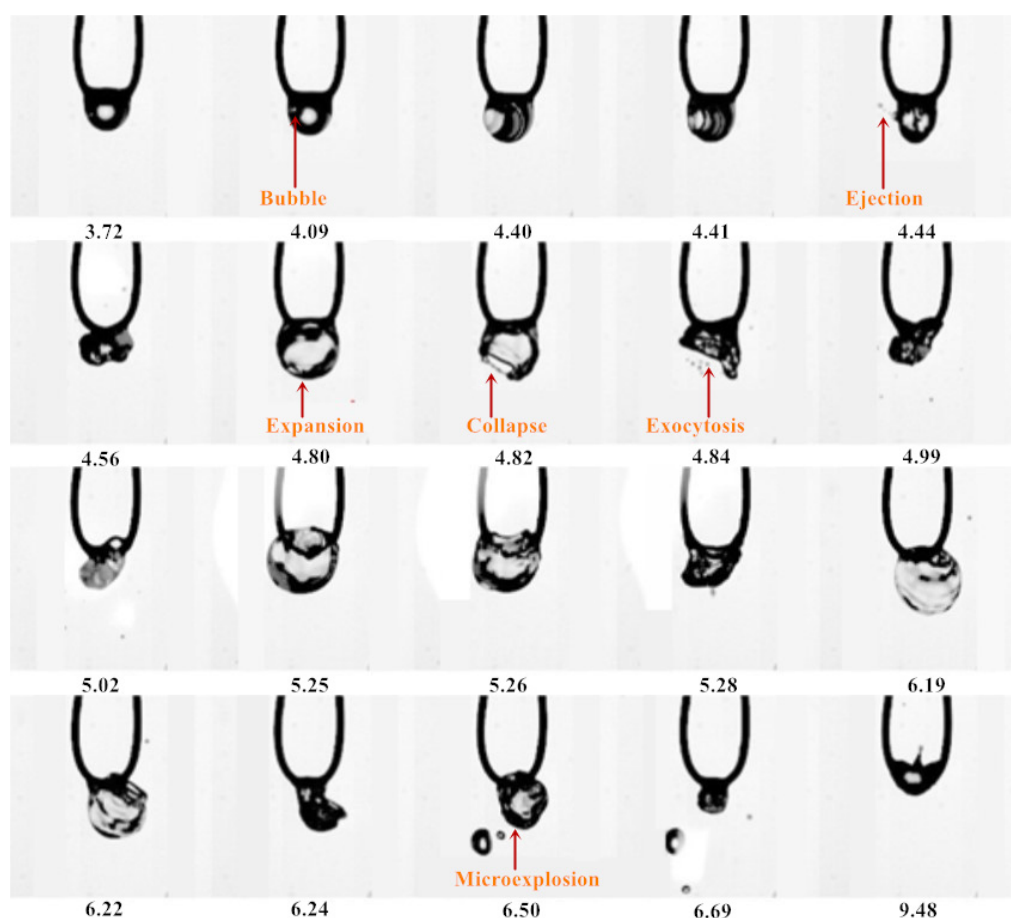


Figure 5. The evaporation sequence diagram of the DE40 droplet.

3.1.3. Evaporation Sequence of the DE60 Droplet

The evaporation sequence diagram of the DE60 droplet is shown in Figure 6. Different from the DE20 and DE40 droplets, the DE60 droplet hung above the filaments because the content of light components was higher than that of heavy components, and the viscosity and surface tension of the droplet were smaller. At the time of 10.27 ms/mm^2 , mass transfer began to appear inside the droplet and the heterogeneous particles moved upward at the transparent place inside the droplet. At 11.85 ms/mm^2 , the bubble volume reached the maximum and the surface of the droplet appeared concave. Then, the bubble burst and the ethanol vapor in the droplet escaped. At 11.90 ms/mm^2 , the droplet produced an ejection phenomenon and the main droplet sputtered out a small droplet. However, the ejection intensity was very low, the heat taken away by the sub-droplets was limited, and

the internal temperature of the droplet had not changed significantly, so the droplet began to expand again soon. At 12.24 ms/mm^2 , it expanded to the maximum value. Subsequently, the droplet produced a relatively weak ejection phenomenon and the ethanol vapor in the bubble was released. At 12.65 ms/mm^2 , the droplet was divided into three main parts. Although each part had a nucleation point, the nucleation internal pressure was less than the surface tension of the liquid film, and the gas could not escape through the surface of the liquid film, so the three parts gradually merged, the nucleation points gradually gathered, and the droplet started to expand. At 22.10 ms/mm^2 , the droplet produced a very strong edge explosion, the whole droplet exploded into numerous sub-droplets, and the main droplet also expanded into a plane shape. After the main droplet stabilized, the vapor cloud phenomenon was observed at 24.06 ms/mm^2 . The vapor cloud was formed because the bubbles generated around the heterogeneous nucleation point in the droplet gradually moved to the droplet surface under the action of internal circulation, which accelerated the evaporation rate on the droplet surface and formed a vapor (fuel vapor)–gas (ambient gas) mixture near the droplet. The non-uniform heating of the steam–gas mixture in the environment led to non-isothermal condensation, which made part of the steam condense into a liquid state. The steam cloud was mainly produced in the later stage of evaporation, in which the content of light component fuel in droplets was low and the material composition was mainly heavy component fuel, so the steam density produced was high.

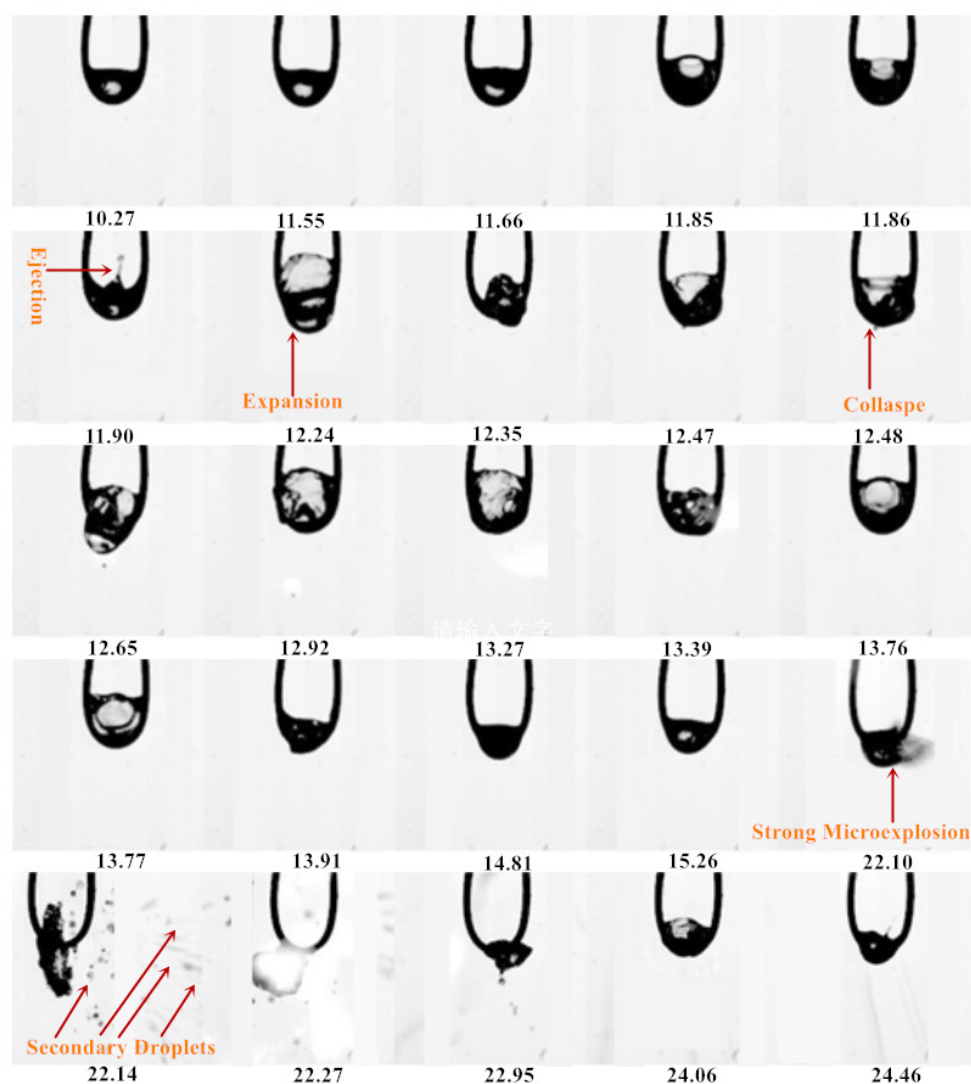


Figure 6. The evaporation sequence diagram of the DE60 droplet.

3.1.4. Evaporation Sequence of the DE80 Droplet

The evaporation sequence diagram of the DE80 droplet is shown in Figure 7. Among the DE80 droplet, the proportion of light component fuel ethanol was extremely high. Unlike the previous water-in-oil droplets, the DE80 mixed droplets were oil-in-water droplets, in which a large amount of ethanol was wrapped around diesel. Because the boiling point of ethanol was lower than that of diesel, the diesel inside the droplet did not change in the early heating process and the ethanol in the coating gradually evaporated. Because of the large volume fraction of ethanol, the evaporation of ethanol on the droplet surface took away the heat of the droplet, so there was no obvious change in the droplet for a long time, except for the fact that the volume decreased gradually. At 21.66 ms/mm², the droplet began to fluctuate and, in the subsequent process, it could be seen that the droplet surface experienced severe ejection. This was because the temperature of the droplets reached the boiling point of ethanol, the droplet started to boil, and small droplets were sprayed out. At 23.66 ms/mm², the droplet expanded to the maximum value, then the droplet underwent severe deformation, and the liquid filament produced by deformation was broken under the action of tensile force. At the time of 23.70 ms/mm², the droplet contracted into a sphere with several obvious bubbles in it. In the ensuing time, the ethanol content in the droplets gradually decreased and the droplet encapsulation mode changed to water-in-oil droplets. The droplet expanded and sprayed several times in succession until it disappeared.

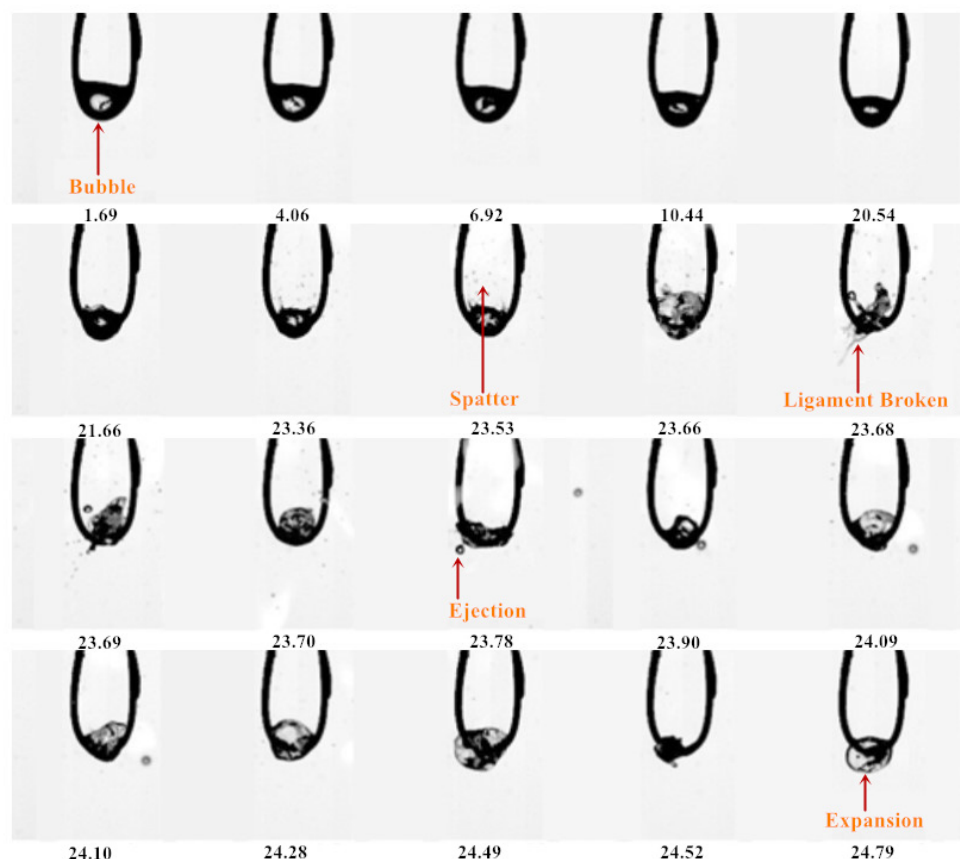


Figure 7. The evaporation sequence diagram of the DE80 droplet.

3.2. Evaporation Mode

According to the evaporation sequence diagram of several ethanol–diesel droplets with different mixing ratios in Section 3.1, and the evaporation modes shown in Figure 8, the following evaporation modes were summarized: (1) The strong micro-explosion mode. In the evaporation process of the DE20 droplet and the DE60 droplet, a strong micro-explosion

evaporation mode was produced. Before the strong micro-explosion evaporation mode, the droplets all experienced stable combustion for a period of time and the heterogeneous nucleation points gradually gathered on the surface of the droplet. After the temperature reached the overheat limit, the droplet suddenly exploded at a certain moment, bursting out countless sub-droplets. The ignition of sub-droplets could reduce the ignition delay time and facilitate the engine starting. In addition, the DE60 droplet experienced a long period of fluctuating evaporation before combustion and the ethanol concentration in the droplets decreased a lot. Therefore, the sudden explosion mode will only occur when the ethanol concentration is not high and a large amount of heat is accumulated. (2) The ejection mode. The ejection mode occurred in the evaporation process of ethanol and diesel oil with different blending ratios. The heterogeneous nucleation point moved to the vicinity of the droplet surface and the bubble internal pressure increased gradually. However, due to the low content of light components, only one liquid column and several sub-droplets were ejected at this place. The ejection mode had relatively little influence on the whole droplet, but this phenomenon often occurred frequently. (3) The exocytosis mode. The exocytosis mode occurred because the heterogeneous nucleation points in the droplet were evenly distributed and the droplet expanded as a whole, after being heated. Mass transfer occurred inside the droplet and eventually a crater was formed at the weak part of the liquid film surface. Steam and small droplets escaped from the crater and the resulting counter-impact force made the droplet fluctuate violently, but there was no obvious rule in the formation position of the crater. (4) The tensile crushing mode. This mode mainly occurred after the sharp deformation of the droplet, the heterogeneous nucleation points were roughly distributed in a straight line, the droplet was stretched into an irregular strip structure as a whole, and it was then split into several sub-droplets with different sizes.

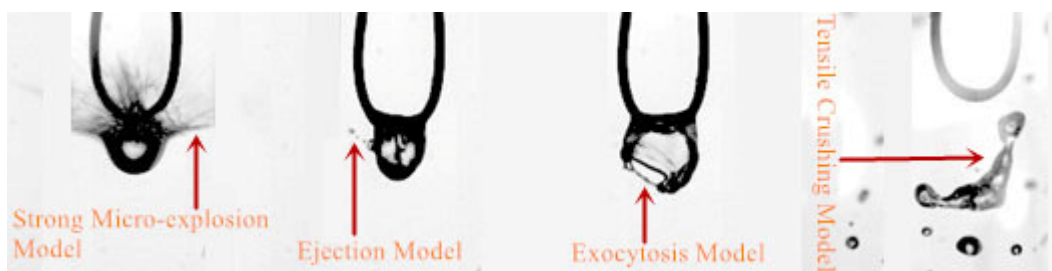


Figure 8. Evaporation mode.

In comparison, the strong micro-explosion mode was more intense, which produced more small droplets and accelerated fuel combustion. In addition, the droplet expanded into a plane and then returned to a spherical shape, drawing more air, which was beneficial to the full mixing of oil and gas. In the exocytosis mode, the gas in the droplet escaped and the reaction force on the droplet made the droplet deform violently and break. The explosion intensity of ejection mode was very low, which had little influence on the whole droplet. The sub-droplet ejected from the droplet could catch fire quickly after escaping, because of its small volume and light component steam, thus reducing the ignition delay time. Different evaporation modes occurred in the heating process of mixed droplets with the same components and different proportions, because the droplets produced different ejection and micro-explosion phenomena. The micro-explosion of droplets was related to the difference in the boiling point of the mixed fuel and also the surface tension and curvature of heavy components.

According to the Young–Laplace equation:

$$\Delta p = p_1 - p_2 = 2\sigma H \quad (1)$$

where P_1 represents the pressure at the concave surface of the droplet, P_2 represents the pressure at the convex surface of the curved surface, σ represents the surface tension, and H

represents curvature. Therefore, only when the pressure generated by the light component steam inside the mixed droplet rapidly exceeded the sum of atmospheric pressure and the pressure generated by the heavy component fuel wrapped outside, could a strong micro-explosion occur; otherwise, the steam inside the droplet could only squeeze the droplet to appear as a small hole to cause ejection or exocytosis.

3.3. The Influence of Mix Proportion on the Droplet Diameter

The change curve of normalized diameter of ethanol–diesel droplets with different mixing ratios with time is shown in Figure 9. It could be seen from Figure 9a that although diesel was a composite component, it did not fluctuate greatly during evaporation and the droplet diameter changed smoothly with time, which basically conformed to the D^2 law [48] of single-component droplet evaporation, as follows: After entering the high temperature environment, the droplet evaporated slowly due to heating, the diameter decreased gradually, and the evaporation rate was almost constant.

$$\frac{d^2}{d_0^2} = 1 - K \frac{t}{d_0^2} \tag{2}$$

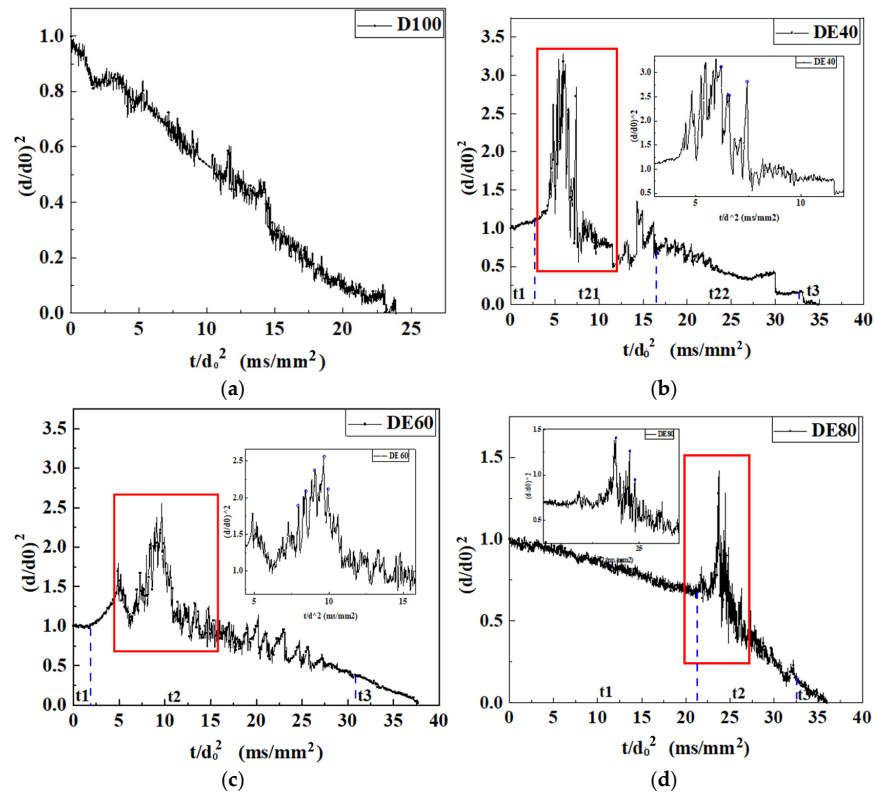


Figure 9. The change curve of the normalized diameter of ethanol–diesel mixed droplets with different mixing ratios with time. The red box is the area that needs to be enlarged. The dash lines is the start or end time of fluctuating evaporation. (a) The curve of the normalized square diameter of the DE100 droplet changes with normalized time. (b) The curve of the normalized square diameter of the DE40 droplet changes with normalized time. (c) The curve of the normalized square diameter of the DE60 droplet changes with normalized time. (d) The curve of the normalized square diameter of the DE80 droplet changes with normalized time.

The parameter K is frequently called the evaporation or burning rate constant. Integrating equation $K = -\frac{d(d_s^2)}{dt}$ yields thereinto $K = -\frac{d(d_s^2)}{dt}$. This is a basic formula that describes the linear decrease in droplet diameter over time. The formula states that the

square of the diameter of the droplet is linear in relation to time and, as the gasification process progresses, the square of the diameter of the droplet decreases linearly with time.

More specifically, the logic behind this formula is based on the assumption that the rate of combustion or vaporization of the droplet is proportional to the surface area of the droplet. Therefore, the K variable in the formula refers to this rate constant, which means that the parameter K is often referred to as the evaporation rate constant or combustion rate constant. Since the integral equation gives Equation (2) in the text, it is shown that the square, d^2 , of the droplet diameter decreases linearly with time, t , where d_0 is the square of the initial diameter and K is the proportionality constant. After adding ethanol to diesel, the diameter of the droplet no longer followed a linear function with time and the evaporation process of the droplet was divided into the following three stages: the heating stage, the fluctuation evaporation stage, and the equilibrium evaporation stage. Similar evaporative combustion [24,49] phenomena have also been reported. They pointed out that the endothermic process of droplets and internal ethanol gasification were the reasons for the three-stage evaporative combustion of ethanol–diesel droplets. In addition, they also found that ethanol–diesel binary fuel exhibited a higher burning rate than pure fuel, which was because fuel could burn destructively during heating; the intensity of this destructive burning was related to the boiling point difference of the fuel that constituted the droplet. Figure 9b shows the curve of the normalized square diameter of the DE40 droplet changing with normalized time. In the heating stage, after the droplet entered the high-temperature environment, the droplet diameter did not decrease, but increased slightly. As the internal temperature rose gradually due to the heat absorption of the droplet, the ethanol in the droplet began to evaporate, while the surface of the droplet was covered with diesel; the vaporized ethanol did not escape, which made the droplet expand gradually. With the continuous heating of the droplet, the internal temperature of the droplet further rose, the ethanol in the droplet reached the overheating limit, and the droplet entered the stage of fluctuating evaporation. Because the fluctuation evaporation stage of DE40 lasted for a long time and the droplet diameter changed greatly during the fluctuation period, it was divided into two stages, as follows: the strong micro-explosion stage and the weak micro-explosion stage. In the stage of strong micro-explosion, a large number of light components in the droplet gathered and the volume of the droplet expanded rapidly, with the maximum diameter reaching 1.81 times the initial diameter. Expansion, ejection, and micro-explosion occurred repeatedly inside and on the surface of the droplet. It could be seen from the local enlarged picture that there were three strong explosions in this stage and the minimum diameter of the droplet was only 0.7 times the initial diameter. After the strong micro-explosion stage, most of the light components in the droplets escaped and the proportion of ethanol remaining in the droplet was very small. Therefore, the ethanol vapor in the droplet was difficult to spray out from the oil film in a strong micro-explosion mode and the evaporation of the droplet entered the weak micro-explosion stage. Small droplets were constantly splashed on the droplet surface, but the droplet diameter fluctuated in a small range. In the equilibrium evaporation stage, the droplet volume was very small, and the droplets on the fibers burned steadily until they burnt out.

Figure 9c shows the curve of the normalized square diameter of the DE60 droplet changing with normalized time. Different from DE40, the diameter of the DE60 droplet decreased slightly in the heating stage, because the ethanol content in the DE60 droplet was relatively high at the initial time and the surface of the droplet was surrounded by light component ethanol. After heating, the ethanol gradually evaporated, which reduced the diameter of the droplet and took away the heat of the droplet. With the continuous heating process, the ethanol inside the droplet began to expand by heating, which offset the decrease in droplet diameter caused by evaporation; meanwhile, the droplet volume gradually expanded and entered the stage of fluctuating evaporation. It could be seen from the local enlarged picture that the DE60 droplet exploded five times in the fluctuation evaporation stage, but, due to the high content of light components, the droplet diameter was still 0.9 times that of the initial diameter at the end of the strong micro-explosion

stage. In the weak micro-explosion stage, the ejection and expansion of the DE60 droplet were more frequent and the intensity was relatively higher. Different from DE40, the DE60 droplet did not explode in the later stage of fluctuation evaporation, but directly entered the equilibrium evaporation stage. In the equilibrium evaporation stage, the light components in the droplet evaporated completely and the droplet volume decreased steadily, which satisfied d^2 law.

Figure 9d shows the curve of the normalized square diameter of the DE80 droplet changing with normalized time. Because the content of light components in the DE80 droplet occupied most of the droplet, the surface of the droplet was mainly ethanol when they were transported to the designated position, showing an oil-in-water mode. Therefore, in the initial stage of heating, the droplet volume did not expand like the DE40 droplet and DE60 droplet, but gradually decreased in the form of a linear function, which conformed to the d^2 law; therefore, it was considered that this stage was the evaporation of pure ethanol. In the fluctuation evaporation stage, the ethanol content in the droplet was already low, the diesel oil covered the surface of the droplet, showing a water-in-oil mode, the droplet began to expand and explode slightly, and there were three strong micro-explosions in this stage. Then, the droplet entered the equilibrium evaporation stage, in which the evaporation of the droplet also satisfied the d^2 law, but the evaporation rate was obviously higher than that of the heating stage. On the one hand, the droplet temperature was higher than the heating stage, on the other hand, the evaporation of droplets was mainly pure diesel. This could be confirmed by calculating the evaporation rates of pure diesel and DE60, which were $0.044 \text{ mm}^2/\text{ms}$, $0.042 \text{ mm}^2/\text{ms}$, and $0.04 \text{ mm}^2/\text{ms}$, respectively.

3.4. Expansion Intensity and Crushing Intensity

In the experimental study of the evaporation of mixed droplets, researchers used the square diameter ratio before and after micro-explosion, to describe the micro-explosion intensity of droplets, as follows:

$$I = \frac{d_0^2}{d_1^2} \quad (3)$$

where d_0 and d_1 were the droplet diameters before and after the micro-explosion. Huang et al. [31] considered that droplets often explode many times during evaporation, so the formula was improved, and the intensity of each explosion was taken into account and then accumulated.

$$I = \sum_{i=0}^n \frac{d_{i0}^2}{d_{i1}^2} \quad (4)$$

Although the equation took every explosion in the life cycle of the droplet into account, the content of each component of the droplet changed greatly after each micro-explosion, and this change was irregular, which made it difficult to explain the micro-explosion intensity of the droplet with a certain mixing ratio. In addition, the above equation did not take time into account, which was also an important parameter for combustion. In view of the above reasons, this paper put forward the concepts of expansion intensity, I_E , and crushing intensity, I_B , as follows:

$$I_E = \frac{\frac{d_1^2}{d_0^2}}{\Delta t_1} \quad (5)$$

$$I_B = \frac{d^*}{\Delta t_2} \quad (6)$$

where Δt_1 was the time from the initial time to the first expansion to the maximum value, Δt_2 was the time before and after the micro-explosion, and d^* was the ratio of the square diameter of the first expansion to the maximum value and the square diameter of the minimum value after the micro-explosion. The higher the expansion intensity of the droplet, the more the light component gasification of the droplet in unit time. The greater

the crushing intensity, the more violent the explosion of the droplet, which was more beneficial to the droplet combustion.

The expansion intensity and crushing intensity of the DE20, DE40, DE60, and DE80 droplets are shown in Figure 10. It can be seen from the figure that with the increase in the blending ratio of ethanol, the expansion intensity and crushing intensity both showed a trend of first increasing and then decreasing. The expansion intensity of the droplet was positively correlated with the crushing intensity. The greater the expansion intensity, the more heterogeneous nucleation points and steam accumulated in the droplet, the higher the pressure in the droplet, and the stronger the crushing. Although increasing the content of light components in droplets increased the internal pressure of droplets, it was known from the Young–Laplace equation that the micro-explosion of droplets was the result of the balance of internal and external pressures. When the content of light components was too high, the liquid film layer was correspondingly thinner, and the pressure that the liquid film bore would also be reduced, thus resulting in the reduction in crushing intensity.

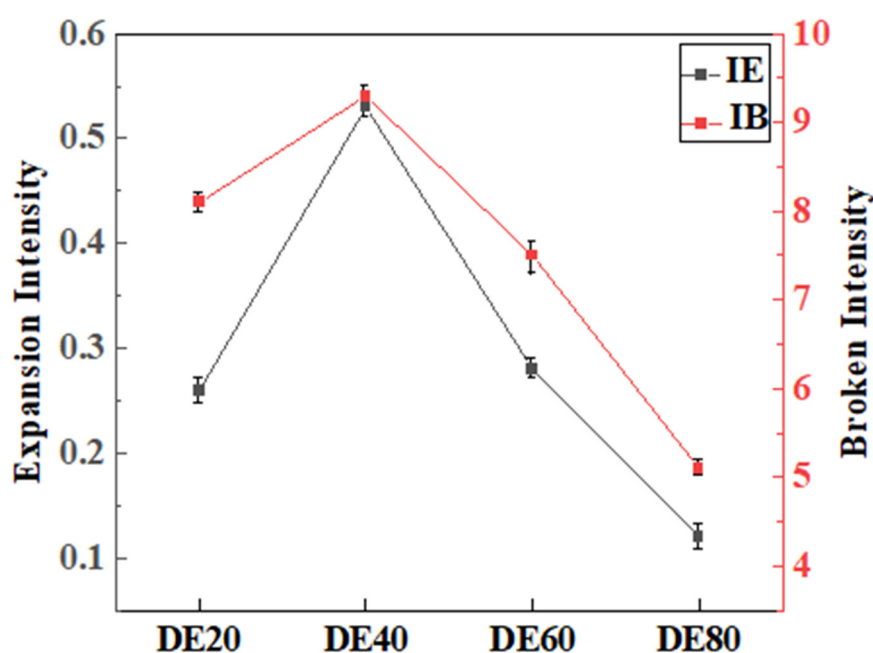


Figure 10. Expansion intensity and crushing intensity of ethanol–diesel droplets with different blending ratios.

3.5. Time Percentage of Different Evaporation Stages

The percentage of ethanol–diesel mixed droplets in different evaporation stages is shown in Figure 11. (The DE20 droplet fell off from the filament after strong micro-explosion and the relevant).

With the increase in ethanol content, the time percentage of the heating stage first decreased and then increased. Because the boiling point of ethanol was much lower than that of diesel, in the heating stage, the increase in ethanol content made the ethanol quickly reach the overheating limit temperature, the ethanol vaporized rapidly, the droplet expanded rapidly, and then the droplet produced strong micro-explosion phenomenon and entered the fluctuation evaporation stage. However, when the content of ethanol reached 80%, the proportion of ethanol was very high, and the droplet was in the mode of ethanol coating diesel, so it was necessary to evaporate a large amount of ethanol on the surface of the droplet before forming an oil film, thus prolonging the time of the heating stage. In addition, the evaporation of a large amount of ethanol in a short time led to the increase in local environmental pressure, which, in turn, made the boiling point rise, which also prolonged the time of the instantaneous heating stage. With the increase in ethanol concentration, the percentage of time in the volatile evaporation stage decreased, and

DE40 accounted for the largest percentage of time in this stage, reaching 88%. In the stage of fluctuation evaporation, the mixed droplet repeatedly produced expansion, ejection, and micro-explosion events, splashing out a number of small-sized sub-droplets. These sub-droplets were easy to ignite because of their small size, which reduced the ignition delay time of the droplet. In addition, the deformation of droplets during crushing was also beneficial to oil–gas mixing and improved the combustion efficiency. Although the initial mixing ratio was different, the components of the three droplets were almost pure diesel in the equilibrium evaporation stage, which was verified by the evaporation rate. According to our experimental results, the DE40 mixture shows the highest destructive intensity during heating, because of its balanced ethanol content, which enhances micro-explosion and evaporation rates. This makes DE40 particularly effective in real engine applications, as it promotes more complete combustion and reduces pollutant emissions. Future research will focus on validating these results under real engine conditions to further validate DE40 as the optimal blend to reduce environmental impact and improve engine performance.

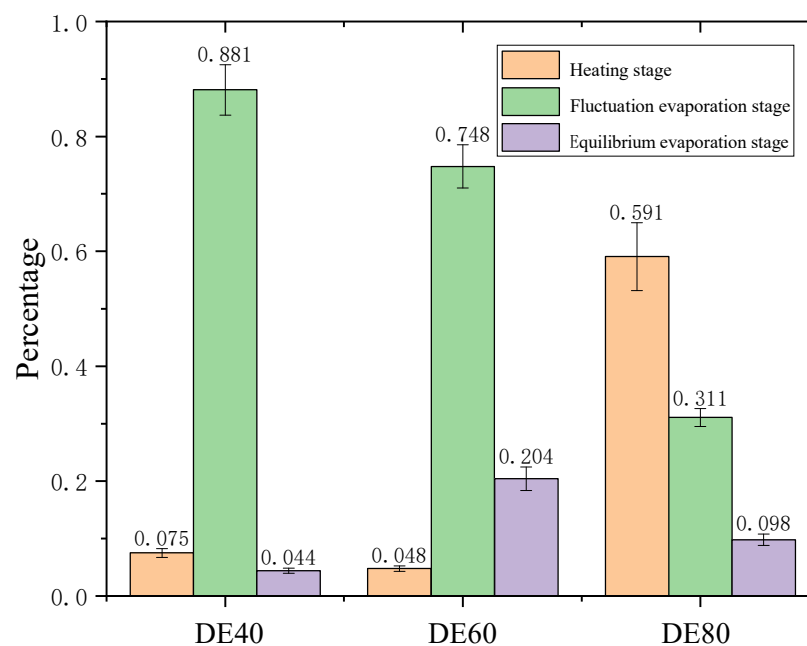


Figure 11. The percentage of different evaporation stages of ethanol–diesel mixed droplets.

4. Conclusions

This study conducted time series chart research and data analysis on the evaporation process of ethanol–diesel mixed droplets with different blending ratios and explored the impact of ethanol blending concentration on the evaporation process of mixed droplets. These studies provide a certain theoretical basis for the future development of alternative fuels for diesel engines and draw the following main conclusions:

- (1) With the increase in ethanol blending ratio in mixed droplets (the proportion of ethanol gradually increased from 20% to 80%), the encapsulation mode of droplets changed from water-in-oil mode to oil-in-water mode. In water-in-oil mode, due to the high content of heavy components, the oil film directly covered the surface of the droplet, and the light components vaporized inside the droplet after they absorbed heat, and then gathered inside the droplet, resulting in ejection and micro-explosion. In the early stage of oil-in-water mixed droplets, light components were wrapped on the surface of the droplet, which needed to undergo evaporation for a period of time and then turned into water-in-oil mixed droplet. The droplet diameter changed in this stage, satisfying the d^2 law.

- (2) The evaporation of droplets was divided into the following four modes: strong micro-explosion mode, ejection mode, exocytosis mode, and tensile crushing mode, and the explosion intensity decreased in turn.
- (3) The vapor cloud phenomenon was found in the evaporation process of the DE60 droplet, which was due to the high evaporation rate on the droplet surface, which led to the mixture of vapor and ambient gas, and the non-isothermal condensation phenomenon of a droplet under the condition of uneven heating.
- (4) Notably, our findings reveal the positive impact of increased ethanol content in reducing emissions such as particulates and NO_x from diesel engines. However, as highlighted in the research by Nord, A.J., J.T. Hwang, and W.F. Northrop [50], while e-diesel can reduce particulate emissions, there remains controversy over its effects on NO_x, CO, and HC emissions. Additionally, the low flash point of e-diesel could pose safety challenges.
- (5) Although diesel is compositionally complex, its evaporation process at 723 K can be regarded as the evaporation of a single-component droplet, satisfying the d^2 law. The evaporation process of ethanol–diesel mixed droplets is divided into three phases, as follows: instantaneous heating, fluctuating evaporation, and equilibrium evaporation stages. During the fluctuating evaporation stage, droplets can produce ejections and micro-explosions of various intensities. The number and velocity of secondary droplets are positively correlated with the expansion and micro-explosion intensities of the droplets; the greater the intensity, the more numerous the secondary droplets.
- (6) Based on the experimental phenomena and comprehensive analysis, a model for the expansion and crushing intensities of mixed fuels was proposed that better conforms to actual laws. This model was used to calculate the expansion and crushing intensities of ethanol–diesel mixed droplets at different blend ratios. With the increase in ethanol blend ratio, both expansion and crushing intensities first increase and then decrease. This trend is consistent with the phenomena observed experimentally, where the expansion and crushing intensities were highest for the DE40 droplets.
- (7) Combining our experiments with those of Chen, Chan-Cheng, and Horng-Jang Liaw [51] comparing typical diesel fuel, we found that ethanol has a significantly higher spontaneous combustion temperature (AIT) of 368.8 °C, which significantly affects the ignition and combustion process under typical engine operating conditions. This higher AIT indicates that the use of ethanol–diesel mixtures may require the adjustment of engine settings or additional preheating measures, to ensure efficient and safe combustion under a variety of environmental conditions. Therefore, the development and optimization of ethanol–diesel mixtures as an alternative fuel requires not only consideration of its environmental properties, but also evaluation of its feasibility and safety in practical applications.
- (8) There is a clear positive correlation between the high microburst intensity observed in this study and the evaporation rate of droplets. Droplets with higher micro-explosion intensity promote more uniform and complete combustion by increasing the contact area between fuel and air. This improved combustion efficiency significantly reduces engine emissions of solid particles and unburned hydrocarbons, making it environmentally friendly. Particularly in internal combustion engines using diesel–ethanol blends, ethanol’s high oxygen content helps to reduce emissions of harmful gases such as nitrogen oxides (NO_x), as the additional oxygen molecules promote a more complete combustion reaction. Future research will use techniques such as spectral analysis to quantitatively analyze this relationship to verify the specific impact between evaporation rate and environmental emissions.

Author Contributions: Conceptualization, Y.Z. methodology, Y.Z. and K.M.; software, Y.Z.; validation, Y.Z. and L.B.; formal analysis, Y.Z.; investigation, Y.Z.; resources, Q.L. and S.P.; data curation, K.M. and L.B.; writing—original draft preparation, Y.Z.; writing—review and editing, Y.Z., K.M., Q.L. and S.P.; visualization, Y.Z.; supervision, Q.L. and S.P.; project administration, K.M. and Q.L.; funding acquisition, Q.L. and S.P. All authors have read and agreed to the published version of the manuscript.

Funding: This work is supported by The University Natural Science Research Project of Anhui Province (No. 2022AH040314).

Institutional Review Board Statement: Not applicable.

Informed Consent Statement: Not applicable.

Data Availability Statement: The data presented in this study are available on request from the corresponding author. The data are not publicly available due to the original computer is lost, the experiment needs to be repeated if the data is needed. Therefore, the data will not be provided without special reasons. If there are special reasons, please apply to the corresponding author.

Conflicts of Interest: The authors declare no conflicts of interest.

References

1. Economics, B.E. *BP Energy Outlook*; BP Plc: London, UK, 2018.
2. Taghizadeh-Alisaraei, A.; Rezaei-Asl, A. The effect of added ethanol to diesel fuel on performance, vibration, combustion and knocking of a CI engine. *Fuel* **2016**, *185*, 718–733. [[CrossRef](#)]
3. Mukhtar, M.; Hagos, F.Y.; Noor, M.; Mamat, R.; Abdullah, A.A. Tri-fuel emulsion with secondary atomization attributes for greener diesel engine—A critical review. *Renew. Sustain. Energy Rev.* **2019**, *111*, 490–506. [[CrossRef](#)]
4. Shi, X.; Pang, X.; Mu, Y.; He, H.; Shuai, S.; Wang, J.; Chen, H.; Li, R. Emission reduction potential of using ethanol–biodiesel–diesel fuel blend on a heavy-duty diesel engine. *Atmos. Environ.* **2006**, *40*, 2567–2574. [[CrossRef](#)]
5. Lee, T.H.; Hansen, A.C.; Li, G.; Lee, T. Effects of isopropanol–butanol–ethanol and diesel fuel blends on combustion characteristics in a constant volume chamber. *Fuel* **2019**, *254*, 115613. [[CrossRef](#)]
6. EL-Seesy, A.I.; Kayatas, Z.; Takayama, R.; He, Z.; Kandasamy, S.; Kosaka, H. Combustion and emission characteristics of RCEM and common rail diesel engine working with diesel fuel and ethanol/hydrous ethanol injected in the intake and exhaust port: Assessment and comparison. *Energy Convers. Manag.* **2020**, *205*, 112453. [[CrossRef](#)]
7. Fernando, S.; Hanna, M. Development of a novel biofuel blend using ethanol–biodiesel–diesel microemulsions: EB-diesel. *Energy Fuels* **2004**, *18*, 1695–1703. [[CrossRef](#)]
8. Abrantes, I.; Ferreira, A.F.; Silva, A.; Costa, M. Sustainable aviation fuels and imminent technologies—CO₂ emissions evolution towards 2050. *J. Clean. Prod.* **2021**, *313*, 127937. [[CrossRef](#)]
9. Hu, Y.-J.; Yang, L.; Cui, H.; Wang, H.; Li, C.; Tang, B.-J. Strategies to Mitigate Carbon Emissions for Sustainable Aviation: A Critical Review From a Life-cycle Perspective. *Sustain. Prod. Consum.* **2022**, *33*, 788–808. [[CrossRef](#)]
10. Li, F.; Tian, J.; Han, K.; Bao, L.; Meng, K.; Lin, Q. Expansion and combustion of droplets that contain long-chain alcohol alternative fuels. *Phys. Fluids* **2021**, *33*, 017117. [[CrossRef](#)]
11. Huang, J.; Wu, Z.; Cai, W.; Berrocal, E.; Aldén, M.; Li, Z. Volume expansion and micro-explosion of combusting iron particles analyzed using magnified holographic imaging. *Powder Technol.* **2023**, *420*, 118412. [[CrossRef](#)]
12. Rao, D.C.K.; Karmakar, S.; Som, S. Puffing and micro-explosion behavior in the combustion of butanol/Jet A-1 and acetone–butanol–ethanol (ABE)/Jet A-1 fuel droplets. *Combust. Sci. Technol.* **2017**, *189*, 1796–1812. [[CrossRef](#)]
13. Rao, D.C.K.; Basu, S. Phenomenology of disruptive breakup mechanism of a levitated evaporating emulsion droplet. *Exp. Therm. Fluid Sci.* **2020**, *115*, 110086.
14. Jing, Q.; Wang, D.; Shi, C. Effects of aluminum powder additives on deflagration and detonation performance of JP-10/DEE mixed fuel under weak and strong ignition conditions. *Appl. Energy* **2023**, *331*, 120477. [[CrossRef](#)]
15. Meng, K.; Huang, Z.; Zhang, X.; Li, L.; Li, R.; Lin, Q. Effect of micro-explosion of biodiesel and ethanol droplets on evaporation: A three-stage mixed fuel droplet evaporation model. *Phys. Fluids* **2022**, *34*, 032113. [[CrossRef](#)]
16. Meng, K.; Li, L.; Zhang, X.; Huang, Z.; Wang, F.; Li, R.; Lin, Q. Comparison of combustion and micro-explosion characteristics of droplet group of biodiesel/ethanol and biodiesel/RP-3/ethanol. *Phys. Fluids* **2022**, *34*, 061903. [[CrossRef](#)]
17. Antonov, D.V.; Fedorenko, R.M.; Strizhak, P.A. Characteristics of child droplets during micro-explosion and puffing of suspension fuel droplets. *Int. J. Heat Mass Transf.* **2023**, *209*, 124106. [[CrossRef](#)]
18. Gallier, S. Aluminum combustion in strong convective flows. *Combust. Flame* **2023**, *249*, 112598. [[CrossRef](#)]
19. Meng, K.; Fu, W.; Lei, Y.; Zhao, D.; Lin, Q.; Wang, G. Study on micro-explosion intensity characteristics of biodiesel, RP-3 and ethanol mixed droplets. *Fuel* **2019**, *256*, 115942. [[CrossRef](#)]
20. Lasheras, J.; Fernandez-Pello, A.; Dryer, F. Experimental observations on the disruptive combustion of free droplets of multicomponent fuels. *Combust. Sci. Technol.* **1980**, *22*, 195–209. [[CrossRef](#)]

21. Li, H.; Rosebrock, C.D.; Wu, Y.; Wriedt, T.; Mädler, L. Single droplet combustion of precursor/solvent solutions for nanoparticle production: Optical diagnostics on single isolated burning droplets with micro-explosions. *Proc. Combust. Inst.* **2019**, *37*, 1203–1211. [[CrossRef](#)]
22. Zhang, X.; Li, T.; Wang, B.; Wei, Y. Superheat limit and micro-explosion in droplets of hydrous ethanol-diesel emulsions at atmospheric pressure and diesel-like conditions. *Energy* **2018**, *154*, 535–543. [[CrossRef](#)]
23. Chao, C.-Y.; Tsai, H.-W.; Pan, K.-L.; Hsieh, C.-W. On the microexplosion mechanisms of burning droplets blended with biodiesel and alcohol. *Combust. Flame* **2019**, *205*, 397–406. [[CrossRef](#)]
24. Botero, M.; Huang, Y.; Zhu, D.; Molina, A.; Law, C. Synergistic combustion of droplets of ethanol, diesel and biodiesel mixtures. *Fuel* **2012**, *94*, 342–347. [[CrossRef](#)]
25. Avulapati, M.M.; Ganippa, L.C.; Xia, J.; Megaritis, A. Puffing and micro-explosion of diesel–biodiesel–ethanol blends. *Fuel* **2016**, *166*, 59–66. [[CrossRef](#)]
26. Yi, P.; Li, T.; Fu, Y.; Xie, S. Transcritical evaporation and micro-explosion of ethanol-diesel droplets under diesel engine-like conditions. *Fuel* **2021**, *284*, 118892. [[CrossRef](#)]
27. Hagos, F.Y.; Aziz, A.R.A.; Tan, I.M. Water-in-diesel emulsion and its micro-explosion phenomenon-review. In Proceedings of the 2011 IEEE 3rd International Conference on Communication Software and Networks, Xi'an, China, 27–29 May 2011; pp. 314–318.
28. Antonov, D.V.; Strizhak, P.A. Heating, evaporation, fragmentation, and breakup of multi-component liquid droplets when heated in air flow. *Chem. Eng. Res. Des.* **2019**, *146*, 22–35. [[CrossRef](#)]
29. Wang, L.; Wang, J.; Qiao, X.; Ju, D.; Lin, Z. Effect of ambient temperature on the micro-explosion characteristics of soybean oil droplet: The phenomenon of evaporation induced vapor cloud. *Int. J. Heat Mass Transf.* **2019**, *139*, 736–746. [[CrossRef](#)]
30. Shinjo, J.; Xia, J. Combustion characteristics of a single decane/ethanol emulsion droplet and a droplet group under puffing conditions. *Proc. Combust. Inst.* **2017**, *36*, 2513–2521. [[CrossRef](#)]
31. Huang, X.; Wang, J.; Yuxin, W.; Qiao, X.; Ju, D.; Sun, C.; Zhang, Q. Experimental study on evaporation and micro-explosion characteristics of biodiesel/n-propanol blended droplet. *Energy* **2020**, *205*, 118031. [[CrossRef](#)]
32. Mikami, M.; Kojima, N. An experimental and modeling study on stochastic aspects of microexplosion of binary-fuel droplets. *Proc. Combust. Inst.* **2002**, *29*, 551–559. [[CrossRef](#)]
33. Zhang, Y.; Huang, Y.; Huang, R.; Huang, S.; Ma, Y.; Xu, S.; Wang, Z. A new puffing model for a droplet of butanol-hexadecane blends. *Appl. Therm. Eng.* **2018**, *133*, 633–644. [[CrossRef](#)]
34. Mishra, D.; Patyal, A. Effects of initial droplet diameter and pressure on burning of ATF gel propellant droplets. *Fuel* **2012**, *95*, 226–233. [[CrossRef](#)]
35. Mikami, M.; Yagi, T.; Kojima, N. *Occurrence Probability of Microexplosion in Droplet Combustion of Miscible Binary Fuels, Symposium (International) on Combustion*; Elsevier: Amsterdam, The Netherlands, 1998; pp. 1933–1941.
36. Meng, K.; Fu, W.; Li, F.; Lei, Y.; Lin, Q. Expansion, injection and micro-explosion phenomena during the full combustion cycle of mixed fuel droplets of ethyl alcohol and biodiesel. *Combust. Theory Model.* **2020**, *24*, 810–828. [[CrossRef](#)]
37. Ismael, M.A.; Aziz, A.R.A.; Mohammed, S.E.; Baharom, M.B.; Hagos, F.Y. Macroscopic and microscopic spray structure of water-in-diesel emulsions. *Energy* **2021**, *223*, 120040. [[CrossRef](#)]
38. Coughlin, B.; Hoxie, A. Combustion characteristics of ternary fuel Blends: Pentanol, butanol and vegetable oil. *Fuel* **2017**, *196*, 488–496. [[CrossRef](#)]
39. Ismael, M.A.; Heikal, M.; Aziz, A.A.; Crua, C.; El-Adawy, M.; Nissar, Z.; Baharom, M.; Zainal, A. Investigation of Puffing and Micro-Explosion of Water-in-Diesel Emulsion Spray Using Shadow Imaging. *Energies* **2018**, *11*, 2281. [[CrossRef](#)]
40. Javed, I.; Baek, S.W.; Waheed, K.; Ali, G.; Cho, S.O. Evaporation characteristics of kerosene droplets with dilute concentrations of ligand-protected aluminum nanoparticles at elevated temperatures. *Combust. Flame* **2013**, *160*, 2955–2963. [[CrossRef](#)]
41. Avulapati, M.M.; Megaritis, T.; Xia, J.; Ganippa, L. Experimental understanding on the dynamics of micro-explosion and puffing in ternary emulsion droplets. *Fuel* **2019**, *239*, 1284–1292. [[CrossRef](#)]
42. Tarlet, D.; Mura, E.; Jossset, C.; Bellettre, J.; Allouis, C.; Massoli, P. Distribution of thermal energy of child-droplets issued from an optimal micro-explosion. *Int. J. Heat Mass Transf.* **2014**, *77*, 1043–1054. [[CrossRef](#)]
43. Valiullin, T.; Vershinina, K.Y.; Kuznetsov, G.; Strizhak, P. An experimental investigation into ignition and combustion of groups of slurry fuel droplets containing high concentrations of water. *Fuel Process. Technol.* **2020**, *210*, 106553. [[CrossRef](#)]
44. Antonov, D.; Shlegel, N.; Strizhak, P. Secondary atomization of gas-saturated liquid droplets as a result of their collisions and micro-explosion. *Chem. Eng. Res. Des.* **2020**, *162*, 200–211. [[CrossRef](#)]
45. Meng, K.; Bao, L.; Shi, Y.; Han, K.; Lin, Q.; Wang, C. Experimental investigation on ignition, combustion and micro-explosion of RP-3, biodiesel and ethanol blended droplets. *Appl. Therm. Eng.* **2020**, *178*, 115649. [[CrossRef](#)]
46. Meng, K.; Bao, L.; Li, F.; Wang, C.; Lin, Q. Experimental understanding on combustion and micro-explosion characteristics of mixed droplets of aviation fuel, biodiesel and ethanol. *J. Energy Inst.* **2021**, *97*, 169–179. [[CrossRef](#)]
47. Mura, E.; Calabria, R.; Califano, V.; Massoli, P.; Bellettre, J. Emulsion droplet micro-explosion: Analysis of two experimental approaches. *Exp. Therm. Fluid Sci.* **2014**, *56*, 69–74. [[CrossRef](#)]
48. Langmuir, I. The Evaporation of Small Spheres. *Phys. Rev.* **1918**, *12*, 368–370. [[CrossRef](#)]
49. Pan, K.-L.; Chiu, M.-C. Droplet combustion of blended fuels with alcohol and biodiesel/diesel in microgravity condition. *Fuel* **2013**, *113*, 757–765. [[CrossRef](#)]

50. Nord, A.J.; Hwang, J.T.; Northrop, W.F. Emissions from a Diesel Engine Operating in a Dual-Fuel Mode Using Port-Fuel Injection of Heated Hydrous Ethanol. In Proceedings of the ASME 2015 Internal Combustion Engine Division Fall Technical Conference ICEF2015 ICEF2015-1067, Houston, TX, USA, 8–11 November 2015.
51. Chen, C.-C.; Liaw, H.-J.; Shu, C.-M.; Hsieh, Y.-C. Autoignition Temperature Data for Methanol, Ethanol, Propanol, 2-Butanol, 1-Butanol, and 2-Methyl-2,4-Pentanediol. *J. Chem. Eng. Data* **2010**, *55*, 5059–5064. [[CrossRef](#)]

Disclaimer/Publisher’s Note: The statements, opinions and data contained in all publications are solely those of the individual author(s) and contributor(s) and not of MDPI and/or the editor(s). MDPI and/or the editor(s) disclaim responsibility for any injury to people or property resulting from any ideas, methods, instructions or products referred to in the content.